

Mixing Characteristics of Kerosene-Lox in a Swirl Injector at 100 bar

Junyoung Heo, Jeongseok Kang, Hong-Gye Sung[†]

*The 4th R&D Institute, Agency for Defense Development
Aerospace and Mechanical Engineering, Korea Aerospace University
KOREA*

[†]E-mail: hgsung@kau.ac.kr

Abstract : The The turbulent mixing characteristics of Kerosene-LOx in a coaxial swirl injector 100 bar have been numerically investigated. Turbulent model is based on large eddy simulation with real-fluid transport and thermodynamics. The effects of equation of state (EOS), chamber pressure are evaluated in a point of the mixing efficiency and pressure fluctuations. The dominant frequency is same as the hairpin vortex shedding frequency generated by film wave at the LOx post.

Key Words : Supercritical, Large Eddy Simulation, Mixing Characteristics, Equation of State, Vortex Shedding Frequency

1. Introduction

A liquid rocket engine for the space launch vehicle is operating at high pressure in order to increase the thrust and combustion efficiency so that its propellants are exposed to supercritical conditions in the combustion chamber. The supercritical condition is the state of the arbitrary substance being enclosed by the environment beyond its critical point. In such conditions, the propellants experience the transition of thermophysical properties differently than during this from phase change process at subcritical conditions. At near the critical point, the engine performance can be achieved with high energy density because propellant properties exhibit gas-

like diffusivities and liquid-like densities. Hence, the study of the mixing and combustion process of the propellants at supercritical conditions is an essential subject.

For understanding the atomization, mixing and combustion phenomena in liquid rocket engine, experimental studies are performed in a wide range of pressures and temperatures, including the supercritical conditions. The Raman scattering technique lately has become the standard diagnostic method for quantitative species detection. Lubarsky et al. performed experiments about the combustion instability in a high pressure air breathing combustor. As the temperature of the fuel increased, it attained a supercritical state. Later, the spray disappeared and the scattered signal could no longer be detected. Also, unstable modes were observed during the transition to supercritical fuel injection [1].

In research of numerical analysis, the results of the mixing and combustion process in shear coaxial injectors using propellants as liquid oxygen/gaseous methane and liquid oxygen/gaseous hydrogen at

Received: April 16, 2016 Revised: June 09, 2016

Accepted: June 12, 2016

†Corresponding Author

Tel:+ 82-10-5275-9196,

E-mail: hgsung@kau.ac.kr

Copyright © The Society for Aerospace System Engineering

supercritical conditions were investigated. Huo and Yang observed the mixing and combustion of liquid oxygen/gaseous methane in a shear injector at supercritical conditions [2]. Giorgi and Leuzzi performed the numerical analysis of mixing and combustion in liquid oxygen/gaseous methane shear coaxial injector at supercritical conditions [3]. Sierra et al. numerically investigated reaction mechanisms and combustion characteristics for the recess number using hydrogen and liquid oxygen as propellants [4]. Hiroshi et al. analyzed nitrogen injection characteristics and compared the numerical results to pressure and temperature in the combustor [5].

In this study, the turbulent mixing of a kerosene/liquid oxygen coaxial swirl injector under supercritical pressures, 100 bar has been numerically investigated. The turbulent numerical model is based on LES with real-fluid transport and thermodynamics; Soave-Redlich-Kwong (SRK) [6], Peng-Robinson (PR) [7], and Redlich-Kwong and Peng-Robinson (RK-PR) [8] equation of state, Chung's model for viscosity/conductivity, and Fuller's theorem for diffusivity to take account for Takahashi's compressible effect.

2. Numerical Method

2.1. Filtered governing equations

The theoretical formulation is based on the filtered Favre averaged mass, momentum, energy, and mixture fraction, f , conservation equations in Cartesian coordinates. The governing equations can be written as:

$$\frac{\partial \bar{\rho}}{\partial t} + \frac{\partial \bar{\rho} \tilde{u}_j}{\partial x_j} = 0$$

$$\frac{\partial \bar{\rho} \tilde{u}_i}{\partial t} + \frac{\partial (\bar{\rho} \tilde{u}_i \tilde{u}_j + \bar{p} \delta_{ij})}{\partial x_j} = \frac{\partial (\bar{\tau}_{ij} - \tau_{ij}^{sgs} + D_{ij}^{sgs})}{\partial x_j}$$

$$\frac{\partial \bar{\rho} \tilde{E}}{\partial t} + \frac{\partial [(\bar{\rho} \tilde{E} + \bar{p}) \tilde{u}_i]}{\partial x_i} = \frac{\partial}{\partial x_i} (\bar{q}_i + \tilde{u}_j \bar{\tau}_{ij} - Q_i^{sgs} - H_i^{sgs} + \sigma_{ij}^{sgs})$$

$$\frac{\partial \bar{\rho} \tilde{f}}{\partial t} + \frac{\partial (\bar{\rho} \tilde{u}_i \tilde{f})}{\partial x_i} = \frac{\partial}{\partial x_i} \left(\bar{\rho} \tilde{D} \frac{\partial \tilde{f}}{\partial x_i} + \Phi_i^{sgs} \right)$$

t , ρ , u , P , E and f are the time, density, velocity, pressure, energy and mixture fraction, respectively. The unclosed sub-grid scale terms are defined

$$\tau_{ij}^{sgs} = \bar{\rho} (u_i u_j - \tilde{u}_i \tilde{u}_j)$$

$$D_{ij}^{sgs} = (\bar{\tau}_{ij} - \tilde{\tau}_{ij})$$

$$Q_i^{sgs} = (\bar{q}_i - \tilde{q}_i)$$

$$H_i^{sgs} = \bar{\rho} (E u_i - E \tilde{u}_i) + (\bar{p} u_i - \bar{p} \tilde{u}_i)$$

$$\sigma_i^{sgs} = (\bar{u}_j \tau_{ij} - \tilde{u}_j \tilde{\tau}_{ij})$$

$$\Phi_i^{sgs} = \bar{\rho} (u_i f - \tilde{u}_i \tilde{f})$$

τ_{ij}^{sgs} , D_{ij}^{sgs} , Q_i^{sgs} , H_i^{sgs} , σ_i^{sgs} and Φ_i^{sgs} are the sgs stress, nonlinearity of viscous stress term, heat flux, energy flux, viscous work, and conserved scalar flux, respectively.

The sgs stress term is modeled with dynamic Smagorinsky model. The subgrid stress τ_{ij}^{sgs} and subtest stress T_{ij} are given by:

$$\tau_{ij}^{sgs} - \frac{\delta_{ij}}{3} \tau_{kk}^{sgs} = -2C_R \bar{\Delta}^2 \bar{\rho} |\tilde{S}| \left(\tilde{S}_{ij} - \frac{\delta_{ij}}{3} \tilde{S}_{ll} \right) = C_R \alpha_{ij}$$

$$T_{ij} - \frac{\delta_{ij}}{3} T_{kk} = -2C_R \hat{\Delta}^2 \hat{\rho} |\tilde{S}| \left(\tilde{S}_{ij} - \frac{\delta_{ij}}{3} \tilde{S}_{ll} \right) = C_R \beta_{ij}$$

where

$$\alpha_{ij} = -2\bar{\Delta}^2 \bar{\rho} |\tilde{S}| \left(\tilde{S}_{ij} - \frac{\delta_{ij}}{3} \tilde{S}_{ll} \right)$$

$$\beta_{ij} = -2\hat{\Delta}^2 \hat{\rho} |\tilde{S}| \left(\tilde{S}_{ij} - \frac{\delta_{ij}}{3} \tilde{S}_{ll} \right)$$

The resolved turbulent stresses, L_{ij} , are defined as:

$$L_{ij} = C_R (\beta_{ij} - \hat{\alpha}_{ij}) + \frac{\delta_{ij}}{3} (T_{kk} - \hat{\tau}_{kk}^{sgs}) = C_R M_{ij} + \frac{\delta_{ij}}{3} L_{kk}$$

where

$$M_{ij} = \beta_{ij} - \hat{\alpha}_{ij}$$

The model coefficient, CR, is suggested by Lilly [9] with a least square method in order to minimize the error:

$$\frac{\partial \langle e_{ij} e_{ij} \rangle}{\partial C_R} = 0$$

where

$$e_{ij} = L_{u_i u_j} - C_R M_{u_i u_j} - \frac{\delta_{ij}}{3} L_{u_k u_k}$$

Then, the model coefficient of SGS stress, C_R , is obtained as:

$$C_R = \frac{L_{u_i u_j} M_{u_i u_j}}{M_{u_k u_k} M_{u_i u_i}}$$

The isotropic model coefficient of SGS stress, C_I , and subtest turbulent stress are modeled as:

$$\hat{\tau}_{kk}^{sgs} = 2C_I \bar{\rho} \Delta^2 |\hat{S}|^2 = C_I \alpha$$

$$T_{kk} = 2C_I \hat{\rho} \Delta^2 |\hat{S}|^2 = C_I \beta$$

The coefficient, C_I , can be calculated in a least-square method to minimize the error:

$$\frac{\partial \langle e_{kk} e_{kk} \rangle}{\partial C_I} = 0$$

where

$$e_{kk} = L_{u_k u_k} - C_I (\beta - \hat{\alpha})$$

Then

$$C_I = \frac{L_{u_k u_k}}{\beta - \hat{\alpha}}$$

Finally, the sgs coefficients, C_R and C_I , are determined dynamically

2.2. Fluid thermodynamics and transport

Ideal and real gas equations of state, such as SRK, Peng-Robinson, and Redlich-Kwong-Peng-Robinson are applied to predict the properties of kerosene surrogate models and study the injection and mixing characteristics in a supercritical swirl injector. A method of Chung is also used for the calculation of transport properties [10].

1. SRK equation of state

SRK equation of state is an improved version of Redlich-Kwong (RK) equation of state considering intermolecular attractive and repulsive forces. The parameters a and b denote the effect of the intermolecular attractive and repulsive force, respectively. α is the third parameter, which is a function of temperature and acentric factor. It includes an additional term which is an acentric factor, ω , that measures uniformity of electric charges' distribution in the molecules.

$$p = \frac{\rho R_u T}{M_w - b\rho} - \frac{a\alpha\rho^2}{M_w(M_w + b)}$$

$$a = \frac{0.42748R_u^2 T_c^2}{p_c} \quad b = \frac{0.08664R_u T_c}{p_c}$$

$$\alpha = \left[1 + (0.48508 + 1.55171\omega - 0.15613\omega^2)(1 - T_r^{0.5}) \right]^2$$

2. PR equation of state

PR equation of state was suggested by Peng and Robinson and aims to analyze states of natural gas systems more accurately. The equation can achieve significantly higher accuracy near the critical point.

$$p = \frac{\rho R_u T}{M_w - b\rho} - \frac{a\alpha\rho^2}{\rho^2 + 2b\rho M_w - b^2\rho^2}$$

$$a = \frac{0.45724R_u^2 T_c^2}{p_c} \quad b = \frac{0.07880R_u T_c}{p_c}$$

$$\alpha = \left[1 + (0.37464 + 1.54226\omega - 0.26992\omega^2)(1 - T_r^{0.5}) \right]^2$$

3. RK-PR equation of state

RK-PR equation of state includes δ_1 and k as functions of each component's critical compressibility factor, Z_c , as well as the acentric factor considered in SRK and PR equations of state. Coefficients related to the terms are represented in Table 1.

$$p = \frac{\rho R_u T}{M_w - b\rho} - \frac{a\alpha\rho^2}{(M_w + \delta_1 b\rho)(M_w + \delta_2 b\rho)}$$

$$a = \left[\frac{3y^2 + 3yd + d^2 + d - 1}{(3y + d - 1)^2} \right] \left(\frac{R_u^2 T_c^2}{p_c} \right)$$

$$b = \left(\frac{1}{3y + d - 1} \right) \left(\frac{R_u T_c}{p_c} \right)$$

$$\alpha = \left(\frac{3}{2 + T_r} \right)^k$$

$$\delta_1 = d_1 + d_2 (d_3 - 1.168Z_c)^{d_4} + d_5 (d_3 - 1.168Z_c)^{d_6}$$

$$\delta_2 = \frac{1 - \delta_1}{1 + \delta_1}$$

$$y = 1 + \left[2(1 + \delta_1) \right]^{\frac{1}{3}} + \left(\frac{4}{1 + \delta_1} \right)^{\frac{1}{3}} \quad d = \frac{1 + \delta_1^2}{1 + \delta_1}$$

$$k = (1.168A_1Z_c + A_0)\omega^2 + (1.168B_1Z_c + B_0)\omega + (1.168C_1Z_c + C_0)$$

Transport properties are predicted by the Chung's model. Mass diffusivity is evaluated using the Fuller's theorem with the Takahashi method.

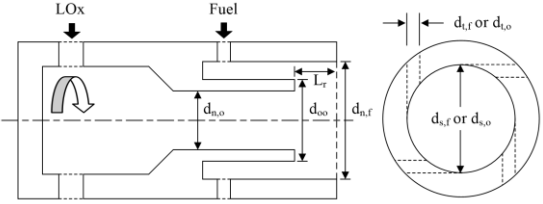
Table 1. Coefficients for estimation of δ_1 and k .

δ_1		k	
d_1	0.428363	A_1	-2.4407
d_2	18.496215	A_0	0.0017
d_3	0.338426	B_1	7.4513
d_4	0.660000	B_0	1.9681
d_5	789.723105	C_1	12.504
d_6	2.512392	C_0	-2.7238

2.3. Numerical scheme

The governing equations are solved by a finite volume method. The spatial discretization is achieved by a fourth order central differencing scheme. The temporal discretization is resolved using a fourth order Runge-Kutta scheme for integration of the real time terms. Pressure decomposition and preconditioning techniques with dual time stepping are applied to circumvent the round-off errors and the convergence difficulties in the momentum equation. The real-gas fluid thermodynamic relation is applied to a preconditioning scheme [11]. The code is paralleled using an MPI library for more effective calculation [12-14].

3. Model Description



$$S_o = \frac{4d_{s,o}d_{n,o}}{\pi n_o d_{t,o}^2} = 1.598, \quad S_f = \frac{4(d_{n,f} - d_{o,o})d_{s,f}}{\pi n_f d_{t,f}^2} = 6.548$$

Fig. 1 Injector geometry and swirl numbers

Table 2. Geometric parameters of an injector

$d_{t,f} / d_{n,o}$	0.3	$d_{o,o} / d_{n,o}$	1.3
$d_{t,o} / d_{n,o}$	0.4	$d_{n,f} / d_{n,o}$	2.0
$d_{s,f} / d_{n,o}$	2.0	n_f	4
$d_{s,o} / d_{n,o}$	1.8	n_o	8

Figure 1 shows the coaxial swirl injector geometry. The swirl numbers of the liquid oxygen and the kerosene are 1.598 and 6.548 respectively. The geometric parameters of the injector are listed in Table 2. The thickness of the LOx post tip is 0.6 mm, and the diameters of LOx and kerosene post are 4.1 and 8.1 mm, respectively. The recess length, L_r , is 3.2 mm. The injector includes three major parts: a tangential inlet, a vortex chamber, and a discharge nozzle. The kerosene (outer) and oxygen (inner) is injected into the swirl injector through the tangential passage. The radial and tangential velocities are determined from the inlet port angle. These velocity components are factors to set the swirl strength and mass flow rate, respectively.

The kerosene model of n-dodecene is applied for this study. Operation and computation conditions are listed in Table 3 and 4, respectively.

Table 3. operating condition

Injector		Coaxial Swirl
Chamber Pressure		100 bar
Fuel		Kerosene; 350K
Oxidizer		Liquid Oxygen; 103K
Mass Flow Rate	Fuel	0.084kg/s
	Oxidizer	0.232kg/s

Table 4. Computation conditions for this study

Case	Equation of state	Chamber pressure, bar	Tangential velocity
1	RK-PR	100	x1
2	SRK	100	x1
3	PR	100	x1

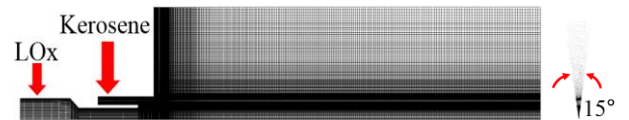


Fig. 2 Computational domain

Quasi-3D flow fields with periodic boundaries are treated herein to save the computational time required for a full 3D calculation, using the large eddy simulation. The tangential inlets, which are circular ports connected to the injector, are approximated with a thin slit. Figure 2 shows a computational domain, divided into 45 blocks which are assigned to 45 processors with 765,000 grids [15]. The turbulent disturbances are applied to the inlet boundary with an intensity of 5% of the mean velocity.

4. Results and Discussion

1. Flow structure

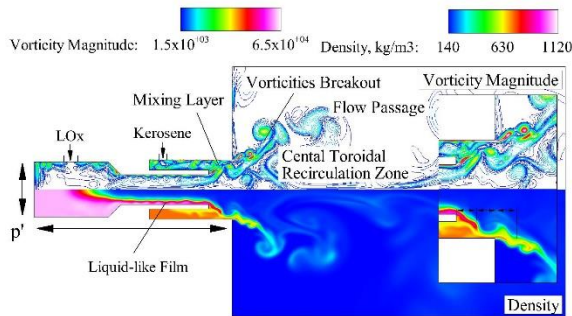


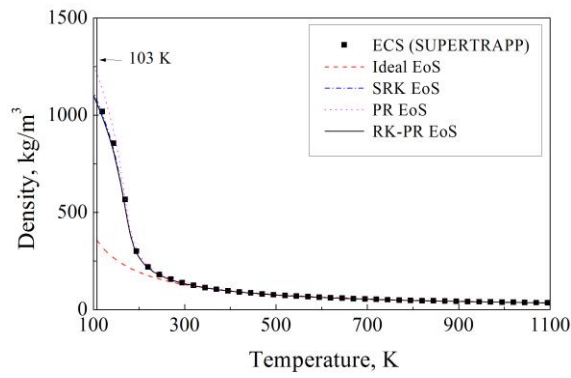
Fig. 3 Vorticity magnitude and turbulent viscosity of a coaxial swirl injector at 100 bar; instantaneous (top) and averaged (bottom) contours

The flow structures of swirl injector computed in this study are presented in Fig. 3. Liquid oxygen and kerosene are introduced into the injector through tangential slots near the injector head. The initial turbulence flow, at the tangential inlet, generates a succession of wavy structures and is convected downstream through the dense liquid oxygen. In a swirl injector, those waves are generated by the presence of oscillations in the chamber or injector post. The strong radial pressure gradient and liquid-like film is formed by centrifugal force. So, the adverse pressure gradient at the exit of the injector gives rise to flow recirculation and finally produces a central toroidal recirculation zone (CTRZ). The shear interaction between oxygen and kerosene near the oxygen/kerosene mixing layer produces the earlier burst of vortices, resulting in enhancement of the mixing of two streams, oxygen and kerosene wavy flow structure generated by the two stream's interaction, with presence oscillations in the

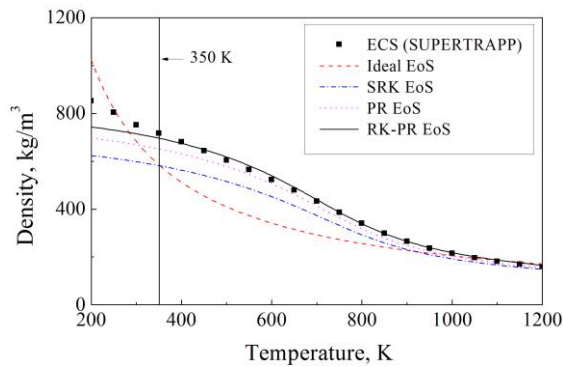
fuel/oxidant feed-line induces the Kelvin-Helmholtz waves at the oxidizer injector post.

A. Effect of real-gas equation of state

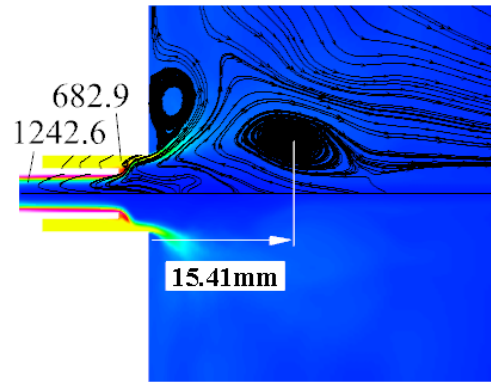
Figure 4 shows the density comparisons of the equation of state models of SRK, PR, and RK-PR, at a wide range of temperature, at 100 bar, supercritical conditions of both kerosene and oxygen. Due to technical difficulties of experiments, to measure the properties under high pressure conditions, these conditions are compared with the results by NIST SUPERTRAPP including the principle of extended corresponding states (ECS). SRK and PR equations of state are usually used to predict the thermophysical properties of real-gas. When kerosene and liquid oxygen are used as propellants, neither the SRK model nor the PR model may be the proper model. The SRK model under-predicts the density for kerosene when compared to the result of the principle of ECS. Whereas the PR model over-predicts the properties for liquid oxygen and has better accuracy than the SRK model. RK-PR model's results of both oxygen and kerosene are, however, similar to those of the principle of ECS, in particular, at the injection temperatures of oxygen and kerosene, 103 K and 350 K, respectively.



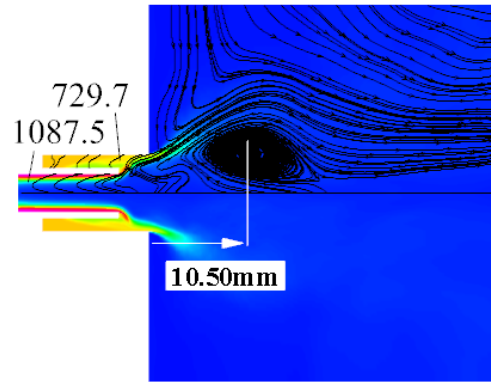
(a)



(b)



(b)PR

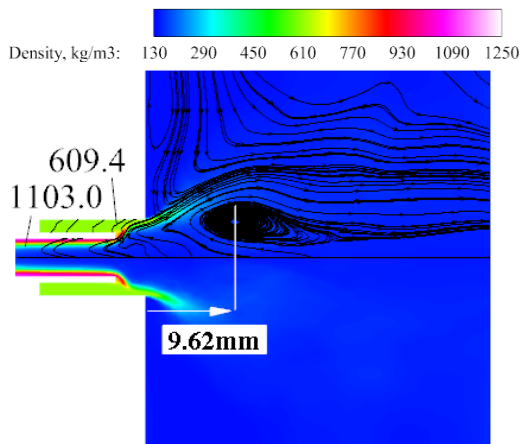


(c)RK-PR

Fig. 4 Density distributions for different equation of state at 100 bar; (a) Oxygen, (b) Kerosene

Fig. 5 Averaged density contours for real-gas equation of states; (a) SRK, (b) PR, (b) RK-PR

$$(\rho_{ECS,Ox} = 1097.1 \text{ kg/m}^3, \rho_{ECS,kerosene} = 750.7 \text{ kg/m}^3)$$



(a)SRK

Figure 5 shows time averaged density fields of a coaxial swirl injector of kerosene and liquid oxygen to the different equations of state with the same inlet conditions. If compared with the ECS principle, $\rho_{ECS,Ox} = 1097.1 \text{ kg/m}^3$ $\rho_{ECS,kerosene} = 750.7 \text{ kg/m}^3$, the SRK and PR models predict lower kerosene density and higher oxygen density respectively. The acoustic waves are transferred back upstream through the CTRZ so that a feedback process occurs and a self-sustained instability phenomenon exists in the region. In the case of the PR model, due to the high density of liquid oxygen, the CTRZ is formed in the rear region relative to the formation in other models. So, the RK-PR equation of state is implemented in the current study due to the best results for kerosene/Lox.

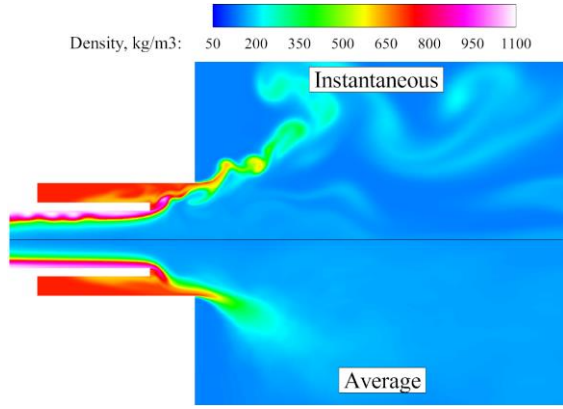


Fig. 6 Density contours at 100 bar; instantaneous (top) and averaged (bottom) contours

Figure 6 represents the instantaneous and averaged density contours at supercritical pressure, 100 bar. The temperatures of LOx and kerosene are 103 K and 350 K respectively. As shown in the figures, the region of phase-change is widely formed due to the supercritical effect.

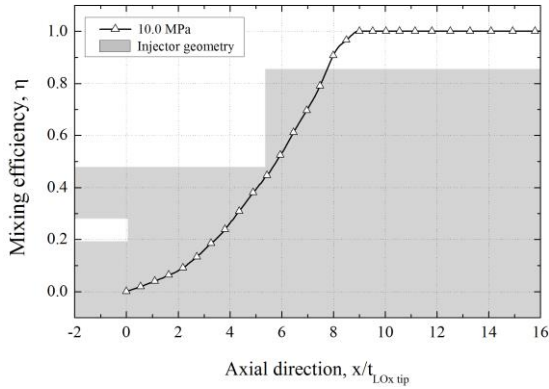


Fig. 7 Mixing efficiency at 100 bar

To quantify the level of mixing, mixing efficiency is considered using the following formula:

$$\eta_{mix}(x) = \frac{\int \rho Y_{Fuel} u \alpha dA}{\int \rho Y_{Fuel} u dA}$$

$$\alpha = \begin{cases} 1 & (\phi_{local} \leq \phi_{global}) \\ \frac{1}{\phi_{local} / \phi_{global}} & (\phi_{local} > \phi_{global}) \end{cases}$$

where ρ and Y_{Fuel} are density and mass fraction of kerosene, respectively. u is the velocity component normal to the area, dA . ϕ_{local} and ϕ_{global} are the local and global equivalence ratio, respectively. The

parameter α is decided by the local equivalence ratio. The mixing efficiency represents how much fuel is spread into the combustion chamber. In other words, the efficiency becomes 1 when the local equivalence ratio is equal to the global equivalence ratio through the whole cross sectional area. Figure 7 shows the time-averaged mixing efficiency. The efficiency increases as it moves downstream after the LOx post, where the mixing starts.

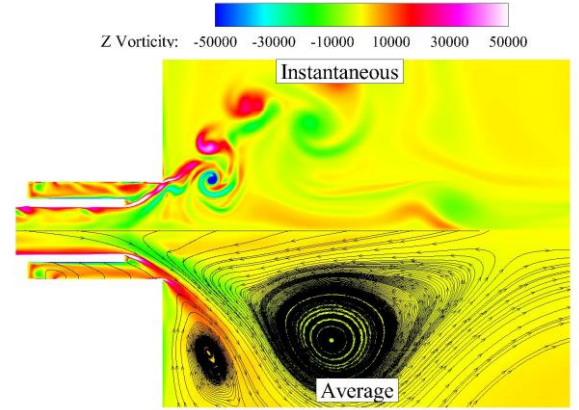


Fig. 8 Z-vorticity contours at 100 bar ; instantaneous (top) and averaged (bottom) contours

Figure 8 shows the instantaneous z -vorticity magnitude. The local vortices are disappeared on the mixing layer due to the rapid vaporization. As a result, the strong toroidal recirculation zone downstream of the injector post is formed.

Figure 9 represents the power spectral densities of the pressure fluctuations at the locations. The Fast Fourier Transform (FFT) technique was implemented for the spectral analysis. Taken as a whole, the frequencies of 2.03–2.07 kHz which is close to Kelvin-Helmholtz frequency. It can be evaluated using the following formula:

$$f_n = St \frac{\bar{U}}{\theta}$$

where, f_n represents the dominant frequency of the hairpin vortex. In turbulent flows, the Strouhal number, St , is 0.046. The mean velocity is 11 m/s near the LOx post tip, and the momentum thickness, θ , is approximately 0.2mm. From this information, the calculated theoretical shedding frequency is 2.53 kHz. These frequencies are weakly dependent on the chamber pressure.

In ideal gases, at a constant temperature, the pressure has no effect on the speed of sound since the pressure and density have opposite effects, and cancel out completely. In non-ideal gases such as this study, the proportion is not exact and the speed of sound slightly depends on pressure conditions

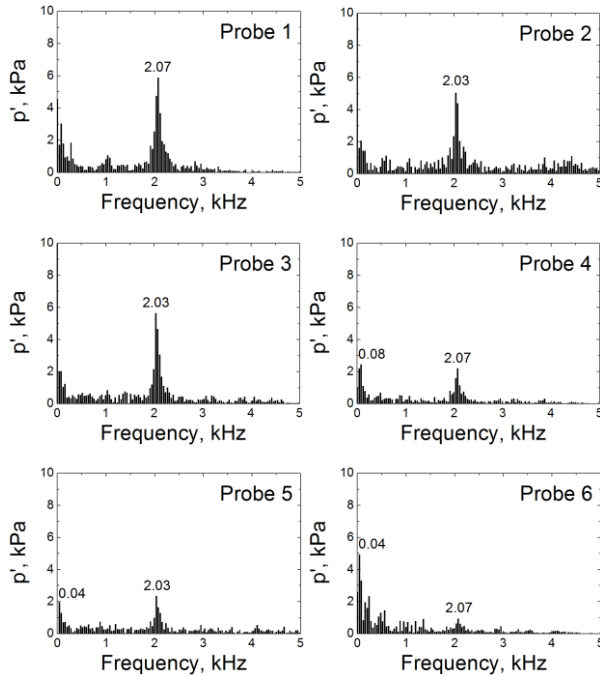


Fig 9. PSD of pressure fluctuations at 100 bar

5. Conclusions

The turbulent mixing of a kerosene-liquid oxygen coaxial swirl injector under supercritical pressure has been numerically investigated. The RK-PR model provides more reasonable thermophysical properties and flow structures than the SRK and PR models. The range of the density field according to the equations of state determines the different size of the CTRZ.

Sinusoidal Kelvin-Helmholtz waves, which are generated by the discharged propellants and the injector wall, develop along the outer wall of the injector. As these waves move downstream, hairpin vortices are magnified. The dominant frequency of 2.03 kHz is the same as these waves

The supercritical environment makes rapid mixing progress. The mixing efficiency reaches the perfect mixing, 1, distinctly faster than transcritical environment. The dominant frequencies of 2.03–2.07

kHz are observed around the injector, which is close Kelvin-Helmholtz frequency.

Acknowledgement

This work was supported by Advanced Research Center Program (NRF-2013R1A5A1073861) through the National Research Foundation of Korea (NRF) grant funded by the Korea government (MSIP) contracted through Advanced Space Propulsion Research Center at Seoul National University.

References

- [1] E. Lubarsky, D. Shcherbik, D. Scarborough, A. Bibik, B. T. Zinn, "Onset of Severe Combustion Instabilities During Transition to Supercritical Liquid Fuel Injection in High Pressure Combustions," 40th AIAA/ASME/SAE/ASEE Joint Propulsion Conference and Exhibit, AIAA Paper No. 2004-4031, 2004.
- [2] H. Huo, V. Yang, "Supercritical LOx/Methane Combustion of a Shear Coaxial Injector," 49th AIAA Aerospace Science Meeting, AIAA Paper No. 2011-326, 2011.
- [3] M. G. D. Giorgi, A. Leuzzi, "CFD Simulation of Mixing and Combustion in LOx/CH₄ Spray Under Supercritical Conditions," 39th AIAA Fluid Dynamics Conference, AIAA Paper No. 2009-4038, 2009.
- [4] P. Sierra, M. Masquelet, S. Menon, "Large-Eddy Simulation of a Reactive Shear Coaxial Injector Configuration," 51st AIAA Aerospace Sciences Meeting, AIAA Paper No. 2013-0563, 2013.
- [5] T. Hiroshi, K. Mitsuo, "Characterization of Cryogenic Nitrogen Jet Mixings under Supercritical Pressures," 51st AIAA Aerospace Sciences Meeting, AIAA Paper No. 2013-0712, 2013.
- [6] G. Soave, "General Circulation Experiments with the Primitive Equations: I. The Basic Experiment," *Chemical Engineering Science* 27, 1197 (1972).
- [7] D. Peng, D. B. Robinson, "A New Two-constant Equation of State," *Industry Engineering Chemical Fundamentals* 15, 59 (1976).
- [8] M. Cismondi, J. Mollerup, "Development and Application of a Three-parameter RK-PR Equation of State," *Fluid Phase Equilibria* 232 74 (2005).

- [9] D. K. Lilly, "A Proposed Modification of the Germano Subgrid Scale Closure Method," *Phys. Fluids A* 4(3), 633 (1992).
- [10] T. Chung, M. Ajlan, L. L. Lee, K. E. Starling, "Generalized Multiparameter Correlation for Nonpolar and Polar Fluid Transport Properties," *Industrial & Engineering Chemistry Research* 27, 671 (1988).
- [11] H. Meng, V. Yang, "A Unified Treatment of General Fluid Thermodynamics and Its Application to a Preconditioning Scheme," *J. Computational Physics* 189(1), 277 (2003).
- [12] J. C. Kim, K. H. Yoo, H. G. Sung, "Large-eddy Simulation and Acoustic Analysis of a Turbulent Flow Field in a Swirl-stabilized Combustor," *J. Mechanical Science and Technology* 25, 2703 (2011).
- [13] K. H. Yoo, J. C. Kim, H. G. Sung, "Effects of Cooling Flow on the Flow Structure and Acoustic Oscillation in a Swirl-stabilized Combustor, Part I. Flow Characteristics," *J. Visualization* 16, 287 (2013).
- [14] H. G. Sung, K. H. Yoo, J. C. Kim, "Effects of Cooling Flow on the Flow Structure and Acoustic Oscillation in a Swirl-stabilized Combustor, Part II. Acoustic Analysis," *J. Visualization* 17, 69 (2014).
- [15] J. Y. Heo, J. S. Hong, H. G. Sung, "Effects of Co Dynamic SGS Model in a Kerosene-Lox Swirl Injector Under Supercritical Condition", *IJASS* 16 pp 254-263 (2015).



Jeongseok Kang

Korea Aerospace University
Large eddy simulation
Supercritical combustion



Hong-gye Sung

Korea Aerospace University
Supersonic mixing and
combustion
Supercritical process
Solid and Liquid rocket

Authors



Junyoung Heo

Korea Aerospace University
Large eddy simulation
Supercritical mixing